



Isolated-core quadrupole excitation of highly excited autoionizing Rydberg states

M. Génévriez ^{*}*Institute of Condensed Matter and Nanosciences, Université catholique de Louvain, BE-1348 Louvain-la-Neuve, Belgium*U. Eichmann [†]*Max-Born-Institute, 12489 Berlin, Germany*

(Received 3 August 2022; revised 9 December 2022; accepted 10 January 2023; published 26 January 2023)

The structure and photoexcitation dynamics of high-lying doubly excited states of the strontium atom with high angular momenta are studied in the vicinity of the $\text{Sr}^+(N = 5)$ threshold. The spectra recorded using resonant multiphoton isolated-core excitation are analyzed with calculations based on configuration interaction with exterior complex scaling, which treats the correlated motion of the two valence electrons of Sr from first principles. The results are rationalized with a model based on multichannel quantum-defect theory and transition dipole moments calculated with a perturbative treatment of electron correlations. Together, both approaches reveal that most of the lines observed in the spectra arise from the interaction of a single optically active state, coupled to the initial state by an electric-dipole transition, with entire doubly excited Rydberg series. The long-range electron correlations responsible for this interaction unexpectedly vanish for identical values of the initial and final principal quantum numbers, a fact related to the quasihydrogenic nature of the high- l Rydberg electron. This special situation, and, in particular, the vanishing interaction, leads to the surprising observation of an electric-*quadrupole* isolated-core excitation with a similar intensity to that of the neighboring electric-dipole transitions.

DOI: [10.1103/PhysRevA.107.012817](https://doi.org/10.1103/PhysRevA.107.012817)

I. INTRODUCTION

Controlling the quantum numbers of high-lying doubly excited (planetary) states in alkaline earth atoms is possible at an unprecedented degree using multistep isolated-core excitation in combination with the Stark switching technique [1–3]. The excitation scheme has enabled successful experimental studies on the transition from independent electron behavior towards strongly correlated electron dynamics in the energy and time domains [4–7]. Interpretation of the complex spectra has been made possible by the development of multichannel quantum-defect theory (MQDT) and R -matrix calculations of short-range parameters, which have proven to be very powerful to extract the key parameters underlying the two-electron dynamics [8,9]. Only recently, calculations based on configuration interaction with exterior complex scaling (CI-ECS) have been introduced to incorporate the increasing extent of electron correlation in configuration space as the core is further excited [10]. This not only provides an improved quantitative description of high-lying doubly excited states but also offers a fascinating visualization of electron correlation in planetary atoms [11].

In this paper we analyze the spectra of a doubly excited Rydberg series of Sr recorded in the vicinity of the $\text{Sr}^+(N = 5)$ threshold with CI-ECS. The theoretical explanation of sections of these spectra, in which an unperturbed autoionizing

Rydberg series attributed to $5gnl$ states [12] is observed despite the absence, at first glance, of dipole coupling to the initial $5dn_i l_i$ state, had initiated a discussion some time ago on how to apply Fano's line-shape theory in this case [13–15]. In this paper we focus on additional striking features in an extended set of experimental spectra, which reveal that the problem is even more complicated than originally discussed. Identifying peculiarities in the dipole transition elements caused by electron correlations, we show how the onset of long-range electronic correlations is responsible for most of the features in the spectra, and how a quadrupole transition at an optical wavelength unexpectedly competes on the same ground as dipole allowed transitions. This latter observation is somewhat unusual since pure quadrupole transitions have been observed only if well isolated from dipole allowed transitions [16] or via interferences in photoelectron angular distributions as a result of the breakdown of the dipole approximation [17,18]. The observation of an isolated-core quadrupole excitation paves ways to control and nondestructively detect Rydberg states by optical manipulation of their ion core [19].

We report experimental spectra that were recorded from $5d_{5/2}n_i(l_i = 12)$ doubly excited states ($n_i = 16$ –21) prepared by multiphoton isolated-core excitation to states in the vicinity of the $\text{Sr}^+(5f)$ and $\text{Sr}^+(5g)$ ionization thresholds, as described in Sec. II. The large-scale CI-ECS approach used to calculate and analyze the spectra is presented in Sec. III, before comparing and discussing the experimental and theoretical results in Sec. IV. The mechanisms underlying electric-dipole excitation to states of predominant $5gnl$

^{*}matthieu.genevriez@uclouvain.be[†]eichmann@mbi-berlin.de

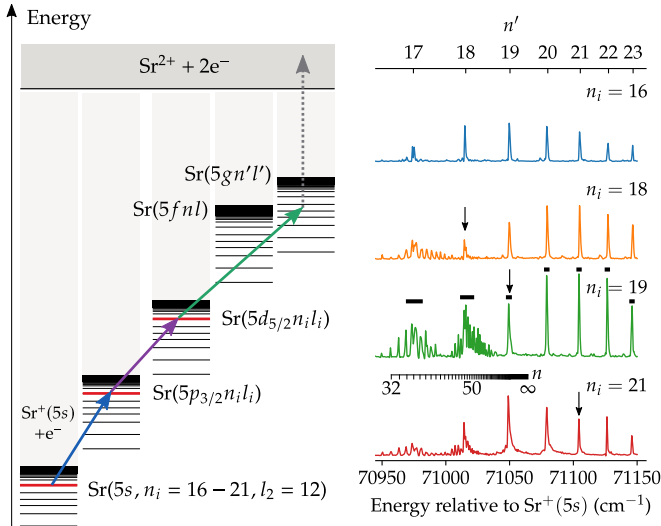


FIG. 1. Left: Multiphoton ICE scheme. Right: Photoionization spectra recorded in the region of the $\text{Sr}^+(5f)$ and $\text{Sr}^+(5g)$ ionization thresholds for $5dn_i l_i$ initial states with $l_i \sim 12$ and $n_i = 16, 18, 19$, and 21 . The assignment bars on the top axis and lower half of the right panel show the principal quantum numbers n' and n relative to the $\text{Sr}^+(5g)$ and $\text{Sr}^+(5f)$ thresholds, respectively. The horizontal solid black lines in the $n_i = 19$ spectrum show the widths of the $5gn'l'$ resonances (see text).

character are elucidated and explained in the light of a simple model, built upon CI-ECS results, combining a four-channel MQDT approach with a perturbative calculation of the transition dipole moments (Sec. IV A). We analyze the earlier discussion on excitation mechanisms [13–15] based on the present results in Sec. IV A 3. The presence of electric-quadrupole excitation in the measured spectra is demonstrated and discussed in Sec. IV B.

II. EXPERIMENT

Excitation of the $5fnl$ and $5gn'l'$ doubly excited Rydberg series follows the well-established sequential resonant multiphoton excitation scheme described elsewhere [2,12,20,21] and shown in Fig. 1. Note that the independent-particle quantum numbers adopted for the state classification are only approximate because of the high degree of electronic correlation. In brief, Sr atoms in an effusive beam are first excited with two dye lasers pumped by an excimer laser from the $5s^2$ ground state via an intermediate resonance to a $5sn_i k_i$ Rydberg Stark state in the presence of a “Stark switching” static electric field. When slowly turning off the field, the Stark state adiabatically evolves into a $5sn_i l_i$ Rydberg state with a value of l_i that is determined by the value of k_i selected upon excitation. The Stark-switching technique thus allows one to prepare the first (outer) electron in a high and selected angular momentum l_i [22]. Nonadiabatic effects as the field is switched off and stray electric fields in the chamber can cause the transfer of a small part of the population to other, neighboring l values [3,11].

About $1.5 \mu\text{s}$ after the excitation of the outer electron, three more dye lasers pumped by a second excimer laser interact

with the inner electron. Lasers 3 and 4 excite the second (inner) valence electron via the $5p_{3/2}n_i l_i$ to the $5d_{5/2}n_i l_i$ resonances (see Fig. 1). A strong fifth laser excites the atom further to the $5fnl/5gn'l'$ series. The pulse energy of the fifth laser is typically around 1 mJ, while the pulse energies of the other dye lasers are kept low ($\sim 10 \mu\text{J}$). Approximately 200 ns after the fifth laser pulse, a detection electric-field pulse (20 ns rise time, 12 kV/cm) is applied. As described in Ref. [21], the detection field together with the photons from the fifth laser photoionize or field-ionize the $5fnl/5gn'l'$ doubly excited states to produce Sr^{2+} ions. These ions are recorded as a function of the photon energy of the fifth laser.

The Sr^{2+} spectra recorded from the $5dn_i(l_i \sim 12)$ doubly excited states with $n_i = 16, 18, 19$, and 21 are shown in the right panel of Fig. 1. The two Rydberg series, converging to the $\text{Sr}^+(5f)$ and $\text{Sr}^+(5g)$ ionization thresholds, are labeled by the assignment bars in the lower and upper parts of the figure, respectively. Although the spectra appear simple at first, more detailed considerations reveal quite the opposite, and there is in fact some debate on the interpretation of the underlying excitation mechanisms [12,14,15,23]. At first glance, the isolated-core-excitation (ICE) approximation [24] does not seem to work in the last step because the $5d - 5g$ core excitation is forbidden by electric-dipole selection rules. Consequently, no $5gn'l'$ line should be observed at all in contrast to the experimental observation. Second, the widths of the $5gn'l'$ lines abruptly reduce when the photon energy is such that the initial and final effective principal quantum numbers of the Rydberg electron are similar, i.e., $n' \simeq n_i$ (vertical arrows in the right panel of Fig. 1). This rapid change is highlighted in the $n_i = 19$ spectrum of Fig. 1, where the horizontal solid black lines show the width of the $5gn'l'$ resonances.

More specifically, for $n' < n_i = 19$ the broad line shape of the $5gn'l'$ states is discernible from the enhanced appearance of the $5fnl$ Rydberg series, where $n \gg n'$, while for $n' \geq 19$, the spectrum consists only of very narrow autoionizing resonances apparently no longer strongly interacting with the $5fnl$ states. When we look at the spectrum $n_i = 21$ of Fig. 1, we clearly observe strong interaction with the $5fnl$ states for $n' < n_i = 21$ and, again, sharp $5gn'l'$ autoionizing resonances for $n' \geq 21$ indicating strongly reduced interaction. Finally, inspecting the spectrum $n_i = 16$ of Fig. 1, we observe only weakly interacting $5gn'l'$ states with $n' > n_i = 16$ throughout the spectrum. Summarizing the observations, we find that the apparent interaction between the $5fnl$ and $5gn'l'$ series is strong for $n' < n_i$ and weaker for $n' \geq n_i$. However, the abrupt change of linewidths (or interaction strengths) cannot be explained by a strong energy dependence of the interaction because, in this case, the change would be independent of n_i .

III. CI-ECS THEORY

To shed light on the mechanisms responsible for $5dn_i l_i - 5gn'l'$ excitation and to understand the origin of the n_i -dependent linewidths, we carried out calculations using the CI-ECS method [10], which treats the motion of the two valence electrons of Sr from first principles. Such calculations go beyond other widely used method because they take long-range electrostatic and exchange interactions between the outer and inner electrons into account and allow the

photoionization cross section to be calculated without relying on the approximations of the ICE model. This is crucial for the high-lying doubly excited states considered here because electron correlations are non-negligible over a large region of configuration space. The large density of states and the large number of channels of the problem make the calculations challenging and require the use of well-optimized basis functions and computational methods (see Refs. [10,11,25,26] for details).

Briefly, a two-electron Hamiltonian describing the valence electrons of Sr is constructed using an empirical model potential for the Sr^{2+} closed-shell core [9]. The Hamiltonian matrix is calculated using a basis of numerical antisymmetrized two-electron functions built from products of two one-electron spin-orbitals. We use exterior complex scaling [27,28] to treat the autoionizing resonances and continuum processes at the heart of the present study. The radial coordinate of each electron is rotated into the complex plane by an angle $\theta = 5^\circ$ for radial distances greater than R_0 , with $R_0 = 150 a_0$ chosen to ensure rapid convergence. The one-electron radial functions are calculated along this complex contour by solving the one-electron Schrödinger equation for the single valence electron of Sr^+ with a finite-element discrete variable representation (FEM-DVR) [29]. The calculation parameters and details can be found in Ref. [11]. In the present work, we used the LS angular-momentum coupling scheme and did not include spin-orbit interaction as it is negligible for electrons in the $\text{Sr}^+(5f)$, $\text{Sr}^+(5g)$, and Rydberg orbitals. We have checked with a restricted basis set that inclusion of spin-orbit interaction leaves the spectra unchanged.

The complex-scaled Hamiltonian matrix has eigenvalues given by $E_i - i\frac{\Gamma_i}{2}$, where E_i and Γ_i are the energies and widths of the eigenstates, respectively. The eigenvalues of states with predominant $5fn(l=12)$, $5gn'(l'=11)$, and $5gn'(l'=13)$ character are shown in Fig. 2 (solid green, blue, and orange circles, respectively). The principal quantum numbers of the discrete Rydberg series converging to the $\text{Sr}^+(5f)$ and $\text{Sr}^+(5g)$ thresholds are shown in the assignment bars. Because the calculations are performed in a box of radius $5300 a_0$, the highest Rydberg state that can be accurately represented is $n \sim 50$. States with higher principal quantum numbers belong to quasicontinua that, above the ionization thresholds, become true (quasidiscretized) ionization continua (solid gray circles). As usual in ECS, the continuum eigenvalues are rotated by approximately -2θ with respect to the real axis. Below the $5f$ threshold, the widths of the states are too small to be visible on the scale of the figure. Their sharp increase immediately above the $5f$ threshold correlates with the opening of the $5f\epsilon l$ channels and indicates that autoionization of $5gn'l'$ states proceeds predominantly into $5f\epsilon l$ continua. The interaction between the $5fnl$ and $5gn'l'$ channels is thus large, as was already observed in the experimental spectra (Sec. II). Above the $\text{Sr}^+(5f)$ threshold, the widths of the members of each series decay smoothly as n^{-3} , and their energies follow Rydberg's formula.

The photoionization cross section σ is calculated from the complex-scaled two-electron wave functions obtained after diagonalization of the complex-scaled Hamiltonian, as described in Refs. [25,30]. Calculations are performed for each possible term of the $5dn_i(l_i = 12)$ initial configuration, which

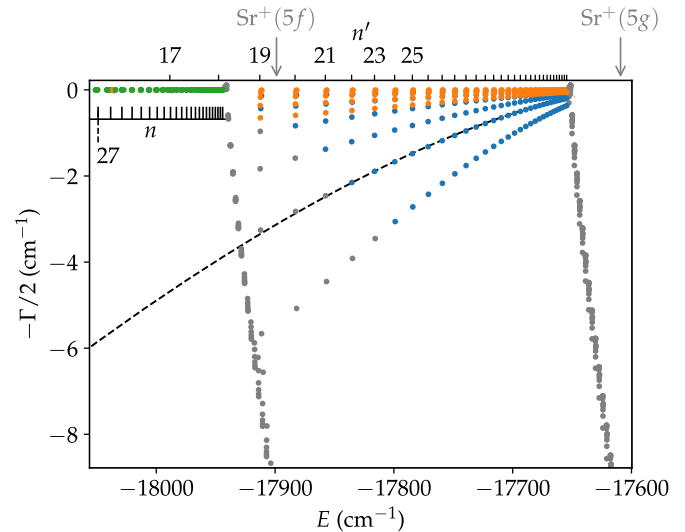


FIG. 2. Energies relative to Sr^{2+} and widths of autoionizing states with predominant $5fn(l=12)$, $5gn'(l'=11)$, and $5gn'(l'=13)$ character (solid green, blue, and orange circles, respectively) calculated with CI-ECS for all possible L values. The dashed curve shows the n^{-3} scaling of the autoionization rates above the $\text{Sr}^+(5f)$ threshold. The upper horizontal axis shows the principal quantum numbers n' relative to the $5g$ ionization threshold and the positions of the $5f$ and $5g$ thresholds. The lower assignment bar shows the principal quantum numbers n relative to the $5f$ threshold. The solid gray circles are continuum states (see text).

is further assumed to be nonautoionizing. The spectra are then obtained by averaging the cross sections, by convolving them with a Gaussian function (full width at half maximum of 0.5 cm^{-1}) to simulate the effect of the laser bandwidth, by including a slight saturation effect [11] (see also Sec. IV A 2), and by shifting them horizontally by the difference (-20 cm^{-1}) between the experimental $\text{Sr}^+(5d_{5/2} - 5g)$ and calculated $\text{Sr}^+(5d - 5g)$ energy splittings.

IV. RESULTS

The spectrum calculated within the electric-dipole approximation for an initial state with $n_i = 19$ and $l_i = 12$ is shown in Fig. 3(a) and compares well with the experimental spectrum in terms of both linewidths and positions. In particular, the abrupt reduction of the linewidth for $n' > 19$ is reproduced. The line at $n' = n_i = 19$ is, however, not reproduced by the calculation, a point that is central to this paper and to which we shall come back in Sec. IV B.

Analysis of the CI-ECS data reveals that, for $n' < n_i$, $5gn'l'$ states with $l' = l_i - 1$ are predominantly excited whereas excitation to $l' = l_i + 1$ states dominates for $n' > n_i$. Because the calculated autoionization rates of the $l_i - 1$ states are larger than those of $l_i + 1$ states by typically one order of magnitude (see Fig. 2), the $5gn'l'$ lines must show larger widths for $n' < n_i$ than for $n' > n_i$, as observed in the experimental and theoretical spectra (see Figs. 1 and 3). Discrepancies between the theoretical and experimental line intensities can be attributed to the fact that CI-ECS calculates the Sr^+ ionization rate whereas the experiment records Sr^{2+} ions produced via two different photoionization and field-ionization

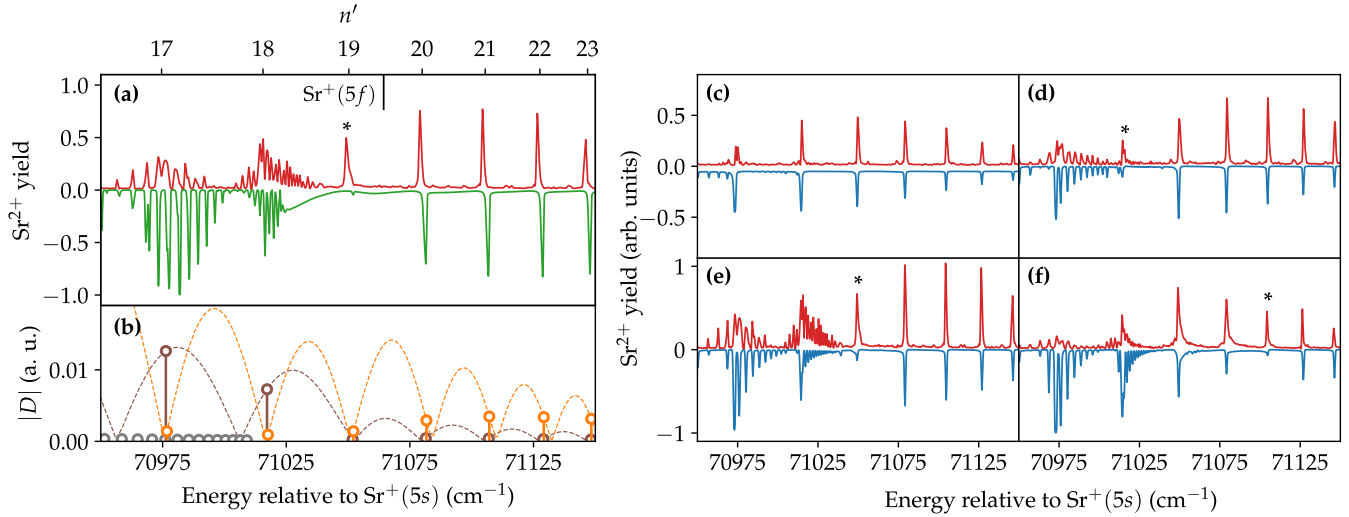


FIG. 3. (a) Comparison between the experimental spectrum (red curve) and the spectrum calculated with CI-ECS (green curve) for $n_i = 19$ and $l_i = 12$. The theoretical spectrum is plotted on a negative scale for clarity. (b) Absolute values of the energy-dependent transition dipole moments D in atomic units (dashed curves) from an initial state with $n_i = 19$, $l_i = 12$ to final states with $n' = 17$ – 23 and with $l' = 11$ (brown) and $l' = 13$ (orange), respectively. Brown and orange circles show the values of $|D|$ at the position of the $5gn'l'$ Rydberg states [assignment bar at the top of (a)], and gray circles show the ICE transition dipole moments to $5fnl$ states with $n = 30$ – 45 and $l = 12$ for comparison. (c), (d), (e), and (f) Comparison of the experimental spectra (red curves) for $n_i = 16$, 18 , 19 , and 21 , respectively, and the results of the four-channel MQDT analysis (blue curves). The positions of quadrupole transitions, neglected in the calculations shown in this figure, are marked by asterisks.

mechanisms with unequal efficiencies below and above the $\text{Sr}^+(5f)$ threshold [21]. This difference is nonetheless insufficient to explain why the CI-ECS spectra do not reproduce the line in the experimental spectra at $n' = n_i = 19$ [asterisk in Fig. 3(a)].

A. Non-ICE electric-dipole excitation

Before tackling the problem of the vanishing line, we elucidate the mechanism responsible for excitation from $5dn_i l_i$ to $5gn'(l' = l_i \pm 1)$ states with $n_i \neq n'$. A two-channel model based on Fano's treatment of photoionization [13] was suggested to explain excitation to $5gn'l'$ states [15,23]. It rests on the breakdown of the independent-electron approximation and the mixing of $5gn'l'$ states with predominantly $5fnl$ states by the electron-electron repulsion. By explicitly calculating the mixing coefficient, we show that this simple ansatz confirms the vanishing of the line at $n' = n_i$ and, upon inclusion of a third channel, predicts the change of the linewidths with n' observed in the spectra. Atomic units are used throughout this section unless stated otherwise.

1. Qualitative three-channel analysis

For the high l values considered here, the long-range dipole part of the electron-electron repulsion dominates such that $l = l' \pm 1$. Starting from zeroth-order independent-electron wave functions, the mixing coefficient between $5fnl$ states and $5gn'l'$ states is written within first-order perturbation theory as

$$c_{5fnl}^{5gn'l'} = \frac{\langle 5g|r|5f \rangle \langle nl|1/r^2|n'l' \rangle}{E_{5gn'l'} - E_{5fnl}} \mathcal{B}_{5fnl}^{5gn'l'}, \quad (1)$$

where $\mathcal{B}_{5fnl}^{5gn'l'}$ denotes the integrals over angular coordinates, which can be calculated analytically using angular-momentum algebra (see, e.g., Ref. [31]). Because the quantum defects of the $5dn_i l_i$ and $5fnl$ series extracted from the CI-ECS data are small ($\delta \lesssim 0.03$), the $|n_i l_i\rangle$ and $|nl = l_i\rangle$ wave functions are to a very good approximation orthogonal. The photoionization cross section σ of a $5dn_i l_i$ state via the $5gn'l'$ states can thus be written, within the electric-dipole approximation, in the simple form

$$\sigma(\omega) \propto \sum_{l'=l_i-1}^{l_i+1} |c_{5fnl_i}^{5gn'l'} \langle 5f|\hat{\epsilon} \cdot \mathbf{r}|5d \rangle|^2 A_{5g'l'}^2(\omega), \quad (2)$$

where ω is the laser angular frequency. The term $\langle 5f|\hat{\epsilon} \cdot \mathbf{r}|5d \rangle$ is the electric-dipole matrix element of the $\text{Sr}^+(5d - 5f)$ transition. The density of states $A_{5g'l'}^2$ of the channel with orbital angular momentum l' and ion-core state $5g$ consists, to a good approximation, in a series of Lorentzian functions centered around the positions of the $5gn'l'$ Rydberg states.

Compared with the expression of the cross section derived using the ICE approximation [32], the transition dipole moment

$$D = c_{5fnl_i}^{5gn'l'} \langle 5f|\hat{\epsilon} \cdot \mathbf{r}|5d \rangle \quad (3)$$

now depends on the photon energy and on n_i through n' ,

$$1/2n'^2 = \hbar\omega_{5d5g} + 1/2n_i^2 - \hbar\omega, \quad (4)$$

where $\hbar\omega_{5d5g}$ is the $\text{Sr}^+(5d - 5g)$ energy difference. The absolute values of the transition dipole moments D from the $5d19(l_i = 12)$ state to $5gn'l'$ final states with $l' = 11$ and $l' = 13$ are shown in Fig. 3(b) as brown and orange circles, respectively. The dipole moments for $l' = l_i + 1$ and $n' \leq n_i$

are very small, and the same is true for $l' = l_i - 1$ and $n' \geq n_i$. This occurs because, in such cases, the dipole moment changes sign near the energies of the $5gn'l'$ states. The phenomenon, analogous to Cooper minima in photoionization cross sections [33], traces back to the change of sign of the $\langle nl|1/r^2|n'l' \rangle$ matrix element in Eq. (1). It is also similar to the predominance, in hydrogenic oscillator strengths, of $l \rightarrow l + 1$ transitions for $n_i < n'$ and of $l \rightarrow l - 1$ for $n_i > n'$ [34]. For $n' = n_i = 19$, both mixing coefficients $c_{5fnl}^{5gn'l=l\pm 1}$ are very small and would in fact vanish for zero quantum defects because the $\langle nl|1/r^2|nl \pm 1 \rangle$ matrix element is exactly zero for hydrogenic wave functions (see Ref. [35] for a mathematical demonstration).

The three-channel model thus shows that the excitation from $5dn_i l_i$ states to $5gn'l'$ states with $n' \neq n_i$ and $l' = l_i \pm 1$ is enabled by long-range dipole interactions between the electrons. The conspicuous abrupt change in interaction strength visible below and above the $5gn'l'$ states for which $n' = n_i$ is a consequence of (i) the changing strengths of the transition dipole moments involving the $5gn'(l_i - 1)$ and $5gn'(l_i + 1)$ states (see Fig. 3) and (ii) the vastly different interaction strength of the $5gn'l_i + 1$ and $5gn'l_i - 1$ series with the $5fnl$ channels. The $5gn'(l_i - 1)$ states, which have a much larger interaction strength with the $5fnl$ channel and thus a much larger autoionization rate than the $5gn'(l_i + 1)$ states, are predominantly excited for $n' < n_i$, while the weakly interacting $5gn'(l_i + 1)$ states, with low autoionization rates, are favorably excited for $n' > n_i$ (see Fig. 2). In essence, excitation of the strongly interacting states is dominant for $n' < n_i$ while excitation of the weakly interacting states dominates for $n' > n_i$. The energy- and initial-state dependence of the transition moments D is thus responsible for many remarkable properties of the spectra reported here.

2. Four-channel quantum-defect theory analysis

To confirm the above conclusions quantitatively, we use a MQDT approach [36–38], where the two-electron wave function is expanded in terms of collision channels

$$|\Psi\rangle = \sum_k A_k |\Xi_k\rangle |\phi_k\rangle. \quad (5)$$

Here, A_k is the admixture coefficient of the k th channel, Ξ_k denotes the core electron wave function including the angular coordinates of the outer electron (the spin is neglected in our analysis), and ϕ_k is the radial Coulomb wave function. Following the phase-shifted R -matrix MQDT approach of Cooke and Cromer [36], the energy-dependent admixture coefficients A_k are obtained from

$$[\mathbf{R} + \tan(\pi\nu^{(p)})]\mathbf{a} = 0. \quad (6)$$

The “phase-shifted” effective quantum numbers $\nu_k^{(p)}$ and admixture coefficients $a_k^{(p)}$ are defined by $\nu_k^{(p)} = \nu_k + \delta_k$ and $a_k^{(p)} = A_k \cos(\pi\nu_k^{(p)})$, where δ_k is the single-channel quantum defect and ν_k is the effective quantum number defined by $\nu_k = n - \delta_k$. The phase-shifted symmetric matrix \mathbf{R} contains only nondiagonal elements R_{kj} which describe the coupling strength between channels k and j .

To simulate an experimentally observed spectrum, we further need to consider the relevant channel-excitation dipole

moments, which act quasi as filters weighing the contributions of the energy-dependent channel admixtures (see, e.g., Fig. 34 of Ref. [9]). With energy-dependent collision-channel dipole moments D_k , the total excitation cross section in the case of one continuum is thus given by

$$\sigma \propto \left(\sum_k A_k D_k \right)^2, \quad (7)$$

while in the case of many continua we have to take into account the incoherent sum of the contributions to each continuum (see Eq. (15) of Ref. [37]).

In an extension of the three-channel model discussed qualitatively in Sec. IV A 1, we are now in a position to simulate the spectra shown in Fig. 1. We use a four-channel MQDT approach comprising a common continuum channel, the $5fnl$ channel, and the $5gn'(l - 1)$ and $5gn'(l + 1)$ channels, denoted as channels 1, 2, 3, and 4, respectively. Following Eqs. (45)–(47) of Ref. [36], we solved Eq. (6). Below the $\text{Sr}^+(5f)$ ionization limit we have one open and three closed channels, while above the $\text{Sr}^+(5f)$ ionization limit channel 2 becomes open leaving us with two bound and two open channels. We assume that the spectra are dominated by exciting the otherwise inherently non-dipole-allowed $5gn'l'$ channels through the admixture of the particular $5fn_i l_i$ state. We note that this admixture gives rise to the notion that the ionic core is no longer isolated. The energy-dependent dipole moments D_3 and D_4 for the different initial n_i are obtained from Eq. (3). The excitation of the continuum (channel 1) and of the $5fnl$ channel through the dipole allowed ICE process of electron shake-up and shake-off is neglected, thus setting $D_1 = D_2 = 0$. Guided by the CI-ECS calculations, we obtain meaningful numbers for the quantum defects and channel interaction strengths. The best match with the experimental resonance positions is obtained using $\delta_1 = \delta_2 = 0$ and $\delta_3 = \delta_4 = 0.03$. We note, however, that the energy value of the $\text{Sr}^+(5g)$ ionization threshold taken from the literature had to be lowered by 1.8 cm^{-1} to get the best overall agreement. The different interaction strengths of the two $5gn'l'$ channels (channels 3 and 4) with the $5fnl$ channel (channel 2) are best incorporated using $R_{23} = 0.1$ and $R_{24} = 0.4$, which reflects the interaction strengths calculated using the CI-ECS method. The other channel interaction strengths are set to $R_{12} = -0.1$ and $R_{13} = R_{14} = 0.1$. The resulting theoretical spectrum is convolved with an effective laser bandwidth (full width at half maximum) of 0.7 cm^{-1} . To account for possible saturation effects, the measured yield can be described by $Y \propto (1 - \exp(-\sigma\Phi))$ [39]. The time-integrated laser fluence Φ in units of photons per unit area is treated here as a fit parameter, which, as it turns out, only slightly affects the line intensities in the final results for states lying below the $5g17l'$ states. In all other cases the measured yield is proportional to the calculated cross section. With this common set of MQDT parameters for the interaction strengths and quantum defects together with the n_i -dependent dipole moments of Eq. (3), we are able to successfully describe the spectra for the four initial $5dn_i l_i$ states, as shown in Figs. 3(c)–3(f). As for CI-ECS, the agreement between the experimental and theoretical MQDT spectra shown in Fig. 3 is excellent, with the exception of the $n' = n_i$ lines marked by the asterisks.

3. Phase-shifted-continuum excitation

In Refs. [12,14] the idea was put forward that the excitation of the $5gnl$ resonances above the $\text{Sr}^+(5f)$ limit proceeds entirely through excitation of a continuum that is locally phase shifted by its interaction with the states of the bound series. This does not require prediagonalization in order to mix the $5fn_i l_i$ state into the $5gn'l'$ states that enables excitation (see discussions in Refs. [14,15]). Within the framework of the four-channel quantum-defect analysis of our spectra presented above, the direct excitation of the $5gn'l'$ channels is no longer possible, but instead, the dipole moment solely emanates from the transition to the $5fnl$ channel. To investigate this interpretation of the spectra, we analyze a simplified quantum-defect-theory model of the $5gnl$ resonances above the $\text{Sr}^+(5f)$ ionization limit, involving only two channels for the sake of clarity. We consider the $5f\epsilon l$ continuum (open channel o) and the $5gnl'$ resonances (bound channel b). The excitation cross section from the initial $5dn_i l_i$ is obtained from Eq. (7) by setting $D_b = 0$, since the excitation of the $5gnl'$ states from the initial $5dn_i l_i$ states is dipole forbidden. The cross section is solely given by the excitation of the continuum channel

$$\sigma \propto A_o^2 D_o^2, \quad (8)$$

where the dipole moment D_o of the transition is given by

$$D_o = \langle 5f | \hat{\epsilon} \cdot \mathbf{r} | 5d \rangle \langle \epsilon l | n_i l_i \rangle \propto D_{\text{ion}} \frac{\sin(\pi n_i + \tau)}{E_i - E_f}. \quad (9)$$

We defined $D_{\text{ion}} = \langle 5f | \hat{\epsilon} \cdot \mathbf{r} | 5d \rangle$. The last term is the overlap integral of the initial bound-Rydberg-electron wave function and the final energy-normalized continuum wave function, describing the shake-off of the electron into the continuum [40]. It can be considered an extension of the familiar ICE overlap integral, which contains the initial and final energy-normalized Rydberg-electron wave functions of autoionizing Rydberg states. E_i and E_f are the excitation energies of the $5fn_i l_i$ state and of the final $5f\epsilon l_i$ state, respectively. The negative continuum phase $-\tau$ replaces the quantum defect $\pi \nu_1$ of the bound states of the channel. τ changes by π when crossing an interacting bound state in the continuum ($5gn'l'$), which means that at a given energy the term $\sin(\pi n_i + \tau)$ becomes equal to 1 and the dipole moment becomes large. Following a standard two-channel quantum-defect approach [36,38] detailed in the Appendix, the cross section can be written for $\delta_i = \delta_o = 0$ as

$$\sigma \propto D_{\text{ion}}^2 \frac{R_{ob}^2}{(E_i - E_f)^2} A_b^2 f(v^{(p)}), \quad (10)$$

where $f(v^{(p)}) \simeq 1$ in the extended vicinity of each $5gn'l'$ resonance.

As a matter of fact, the cross section in Eq. (10) describing the excitation of $5g$ states seems to be formally identical to the one obtained from perturbation theory [see Eq. (2)] if one associates the term $\frac{R_{ob}^2}{(E_i - E_f)^2}$ with the square of the mixing coefficient c given by Eq. (1). We note, however, that in MQDT the interaction strength $V_{nn'}$ between two bound states of different channels such as a $5fnl$ state and a $5gn'l'$ state is related to the channel interaction R by $V_{nn'} = -R/\pi (nn')^{3/2}$. It scales smoothly with n and n' and does not account for

vanishing interaction for a particular combination of quantum numbers, as is the case in first-order perturbation theory where the $\langle nl || 1/r^2 || n'l' \rangle$ matrix element is exactly zero for hydrogenic wave functions with $l = l' \pm 1$. Consequently, the vanishing line obtained in perturbation theory is nonexistent in the MQDT approach of the present section. Except for this, both approaches seem to be equivalent and in agreement with experiment, making the use of either approach and physical interpretation a matter of taste. On the other hand, if one extends the analysis to take into account two $5gnl$ channels, the striking change of the dominant excitation to $5gn'(l' = l_i \pm 1)$ states below and above the principal quantum number of the initial $5dn_i l_i$ state will not be present in the phase-shifted-continuum approach as can be inferred from the spectra displayed in the Appendix. According to the phase-shifted-continuum model, both $5gnl'$ channels are excited quasi with the same strength, i.e., the same dipole matrix element, independent of the initial $5dn_i l_i$ state. Since the full CI-ECS calculations confirm the existence of the vanishing line and also reproduce the striking change of excitation dynamics for quantum number $n' < n_i$ and $n' > n_i$, the mixing of $5fn_i l_i$ character into the $5gn'l'$ channels to allow for dipole excitation seems to be the favored approach.

In essence, the differences between the approaches of Sec. IV A 2 and of the present section are due to the choice of transition dipole moment, which, in particular through the vanishing admixture of $5fn_i l_i$ character to $5gn_i l'$ states, has a major effect as it filters some of the transitions out of the spectra. In contrast, the vanishing admixture has no consequence on the energies and widths of the members of the different series, which smoothly evolve with the principal quantum number (see Fig. 2) and are well described by MQDT. In the approach of the present section, the long-range electron correlations that cause this vanishing were discarded in calculating D_o , and as a result, the vanishing line is not predicted. Such correlations are naturally included in the CI-ECS approach (see Sec. III) and can be incorporated into MQDT by adding a region between the core and exterior regions where close-coupling equations are numerically solved [41]. Alternatively, the model derived in Sec. IV A 2 proposes an *ad hoc* approach where the effect of long-range electron correlations is included only where they play a significant role: in the dipole moments. This way, the spectra are reproduced with a simple set of calculations, albeit much more limited than the aforementioned approaches.

B. Electric-quadrupole ICE

We now consider the $n' = n_i$ lines, for which both theoretical calculations predict weak intensities, in stark contrast to the strong lines observed in the experiment. We found the calculated intensities to be insensitive to the values of the principal quantum number, orbital-angular-momentum quantum number, and quantum defect of the Rydberg electron, a fact suggesting that the discrepancy is not caused by inaccuracies of our wave functions but rather by the omission of an important excitation channel. The spectra in Fig. 3 are calculated within the electric-dipole (E1) approximation, and excitation occurs via the non-ICE mechanism described earlier. However, it is also possible to directly excite the Sr^+

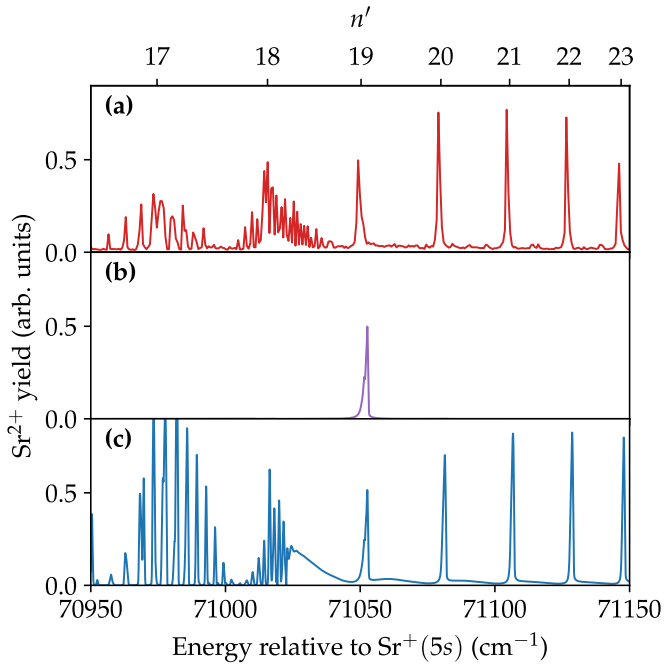


FIG. 4. (a) Experimental and (b) and (c) theoretical CI-ECS spectrum for $n_i = 19$ and $l_i = 12$. (b) shows the contribution of electric-quadrupole transitions to the theoretical spectrum, and (c) shows the total spectrum in which E1 and E2 transitions are summed.

core from the $5d$ state to the $5g$ state by an electric-quadrupole transition (E2). The spectrum resulting from E2 transitions calculated using CI-ECS is shown in Fig. 4(b). It displays a single line around $n' = n_i = 19$ with an amplitude similar to the lines in the E1 spectrum [Fig. 3(a)]. The existence of a single line is well described by the independent-electron ICE model [24] because, for the small quantum defects of the high- l states under consideration, the overlap integral between the initial and final Rydberg-state wave functions entering the cross section is non-negligible for $n' = n_i$ only. Combined together, the E1 and E2 spectra are in excellent agreement with the experimental spectrum (see Fig. 4).

The coexistence of electric-dipole and electric-quadrupole transitions with similar magnitudes is unexpected because quadrupole transitions are typically much weaker [31]. Two facts are at the origin of this remarkable situation. First, the $\text{Sr}^+(5d - 5g)$ E2 transition is particularly intense, and, for example, the associated Einstein A coefficient calculated with our one-electron basis functions [11] reaches 388 s^{-1} . In contrast, the A coefficient of the lower-lying $\text{Sr}^+(5s - 4d_{5/2})$ transition is more than a hundred times smaller ($2.559(10) \text{ s}^{-1}$ [42]). Second, the configuration-mixing coefficients entering the electric-dipole cross section in Eq. (2) have values of $\sim 10^{-2}$, and the E1 transitions are thus 10^4 times less intense than standard E1 transitions.

In cases where the E2 transition is much less intense, one would expect the absence of a line in the spectra at $n = n_i$. This effect is indeed observed in the spectra recorded for the $\text{Sr}(5dn_i l_i - 7dn' l')$ transitions with $l_i = 14$ [43]. In that case, the coefficients of the configuration mixing of $7dn' l'$ states with $6fnl$ and $8pnl$ states are ~ 0.1 [11], whereas the Einstein

A coefficient of the $\text{Sr}^+(5d - 7d)$ E2 transition is 20 s^{-1} . The $\text{Sr}(5dn_i l_i - 7dn' l')$ transitions are thus dominated by the E1 contribution [11] and the expected vanishing of the line at $n' = n_i$ occurs in both experimental and theoretical spectra [10,43].

V. CONCLUSION

We have studied the excitation from $5dn_i l_i$ states to doubly excited states in the vicinity of the $\text{Sr}^+(N = 5)$ threshold. The experimental spectra show the excitation of the ion core from the $5d$ to $5g$ orbitals and exhibit an abrupt change of linewidth at $n' = n_i$. Spectra calculated with CI-ECS fall in excellent agreement with experimental ones and, together with a simple four-channel MQDT model built upon the theoretical data, provide a detailed picture of the complex excitation dynamics of $5dn_i l_i$ states. The electric-dipole excitation to $5gn' l'$ ($n' \neq n_i$) states is made possible by the admixture of $5fn_i l_i$ character due to electron-electron repulsion. The strong energy dependence of the mixing coefficient, and thus of the transition dipole moment, favors excitation to $l' = l_i - 1$ for $n' < n_i$ and to $l' = l_i + 1$ for $n' > n_i$. Because of the large difference between the rates of the $l_i - 1$ and $l_i + 1$ series, the width of the lines in the spectra abruptly changes at the transition between these two regions ($n' = n_i$).

Noticeably, the four-channel model and the CI-ECS calculations in the electric-dipole approximation both fail to reproduce the strong line at $n' = n_i$ observed in the experimental spectra. The line is instead attributed to an electric-quadrupole isolated-core excitation from $5dn_i l_i$ states to $5gn_i l_i$ states, which is confirmed by a CI-ECS calculation including E2 contributions. Albeit surprising, the coexistence of E1 and E2 transitions with the same intensity is explained by the large transition quadrupole moment of the $\text{Sr}^+(5d - 5g)$ transition and by the small transition dipole moment due to the weak admixture of $5fn_i l_i$ character into $5gn' l'$ states.

The observation of an electric-quadrupole ICE paves the way for devising core-excitation schemes suitable, particularly, to all-optical manipulations of Rydberg atoms [44–46]. In a recent study, the state of the Rydberg electron of a Sr atom was detected and coherently manipulated in a non-destructive manner with a multiphoton electric-dipole ICE scheme [19]. The scheme relies on a series of four optical transitions to determine the energy difference ΔE between the $4d_{3/2}(|m_j| = 3/2)$ and $4d_{3/2}(|m_j| = 1/2)$ states of the ion core, which is due to weak electrostatic interaction between the core and Rydberg electrons. Because ΔE depends on n , its measurement served to determine the principal quantum number of the Rydberg electron in a nondestructive manner, i.e., without relying on widely used field-ionization techniques. By demonstrating the possibility to carry out electric-quadrupole ICE, the present work suggests that the excitation of the ion core from the $5s_{1/2}$ state to either of the two $4d_{3/2}(|m_j|)$ states can be used to determine the value ΔE and thus of n in a nondestructive manner and with a scheme involving a single photon.

The change of n and l with the non-ICE electric-dipole excitation discussed above also offers a route to modify the state of the Rydberg electron with visible laser light. For $l_i = 12$ and zero quantum defects, the CI mixing coefficients between $4dn' l'$ states and the $5p19l_i$ state calculated using Eq. (1) are

$\sim 10^{-4}$. Electric-dipole excitation from $5s19l_i$ to $4dn'l'$ states is thus suppressed by 10^{-8} compared with $\text{Sr}(5sn_i l_i - 5pn_i l_i)$ excitation, and its intensity is then comparable to that of the $\text{Sr}(5sn_i l_i - 4dn_i l_i)$ E2 transition [47]. In such a case, dipole and quadrupole transitions coexist at a level similar to the one observed in the present spectra. For larger values of n and l , the CI coefficients decrease rapidly, and electric-quadrupole transitions dominate. In a Rydberg-atom quantum simulator, the interaction between neighboring Rydberg atoms strongly depends on n and l [48]. The possibility to change n and l with visible light opens the way to changing these interactions in a spatially resolved manner.

ACKNOWLEDGMENT

The authors gratefully acknowledge C. Rosen for assistance with the measurements.

APPENDIX: MQDT TREATMENT OF PHASE-SHIFTED-CONTINUUM EXCITATION

We start from the equation for the cross section given in Sec. IV A 3,

$$\sigma \propto A_0^2 [D_{\text{ion}} \sin(\pi n_i + \tau) / (E_i - E_f)]^2. \quad (\text{A1})$$

Following the standard two-channel quantum-defect approach [36,38], $A_0^2 = 1$ results from normalization, and the continuum phase τ is given by

$$\tan(-\tau + \pi \delta_o) = R_{ob}^2 / \tan v_b^{(p)}, \quad (\text{A2})$$

where R_{ob} is the interaction strength between the open and bound channel. Inserting Eq. (A2) into Eq. (A1), the cross section reads

$$\sigma \propto \frac{D_{\text{ion}}^2}{(E_i - E_f)^2} \sin^2 [\varphi - \arctan(R_{ob}^2 / \tan v_b^{(p)})], \quad (\text{A3})$$

with $\varphi = \pi(n_i + \delta_o)$. Using $\sin y = \frac{\tan y}{\sqrt{1 + \tan^2 y}}$ and addition formulas for sine functions, it can be rewritten as a Fano-line-shape-like formula

$$\sigma \propto \frac{D_{\text{ion}}^2 \sin^2 \varphi^2 (q + \epsilon)^2}{(E_i - E_f)^2 (1 + \epsilon^2)}, \quad (\text{A4})$$

where $\epsilon = \tan v_b^{(p)} / R_{ob}^2$ and $q = -1 / \tan \varphi$. If one takes $\delta_o = 0$, we can write

$$\sigma \propto D_{\text{ion}}^2 \frac{R_{ob}^2}{(E_i - E_f)^2} \frac{R_{ob}^2}{R_{ob}^4 + \tan^2 v_b^{(p)}}. \quad (\text{A5})$$

This can be rewritten to explicitly contain the spectral density A_b^2 of bound $5gnl$ autoionizing resonances

$$A_b^2 = R_{ob}^2 \frac{1 + \tan^2 v_b^{(p)}}{R_{ob}^4 + \tan^2 v_b^{(p)}} \quad (\text{A6})$$

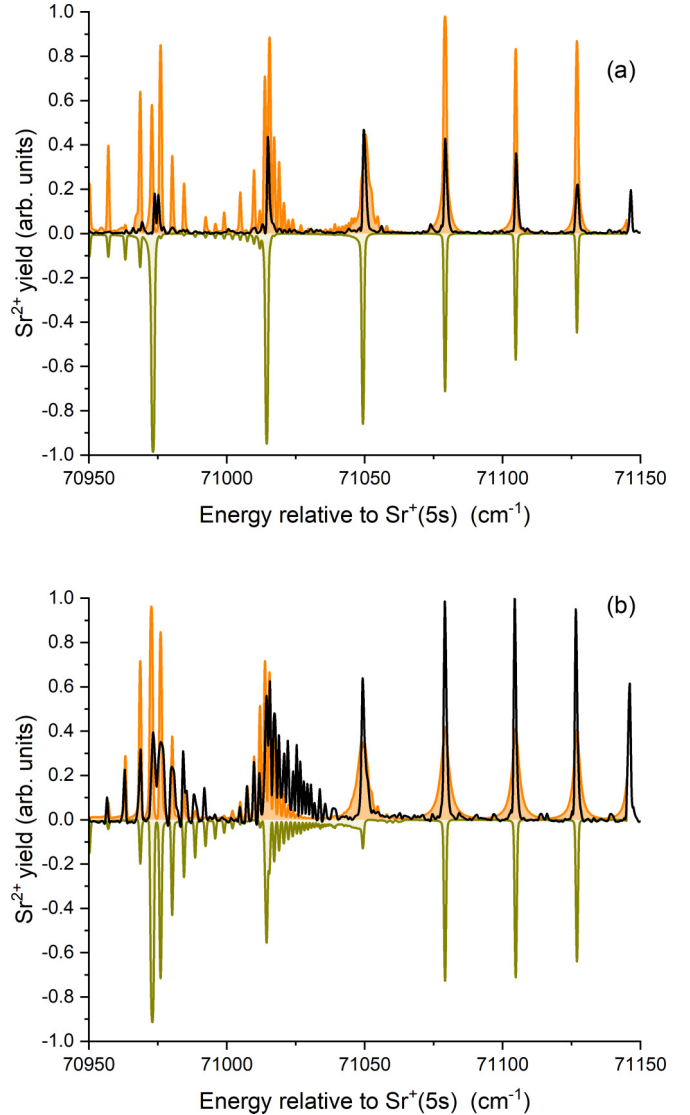


FIG. 5. Spectra of doubly excited states excited from the (a) $5d16n_i (l_i = 12)$ and (b) $5d19n_i (l_i = 12)$ states. Theoretical curves obtained from a five-channel analysis using the MQDT parameters given in Sec. IV A 2: excitation of the $5f$ channel via ICE (shake-up and shake-off excitation) following the model described in Sec. IV A 3 and in the Appendix (orange); excitation through the admixture of the $5fn (l = 12)$ into the two $5g$ channels following the model described in Sec. IV A 2 (green). Experiment: black curves (same as in Fig. 3).

to yield

$$\sigma \propto D_{\text{ion}}^2 \frac{R_{ob}^2}{(E_i - E_f)^2} A_b^2 f(v^{(p)}). \quad (\text{A7})$$

Here, $f(v^{(p)})$ is an analytical function, which is $\simeq 1$ in the extended vicinity of each resonance.

An extension of the model to four channels, as in Sec. IV A 2, is straightforward. The results of the present approach, based on phase-shifted-continuum excitation, are compared with the mixed perturbative and MQDT approach of Sec. IV A 2 in Fig. 5.

- [1] R. R. Jones and T. F. Gallagher, *Phys. Rev. A* **42**, 2655 (1990).
- [2] U. Eichmann, V. Lange, and W. Sandner, *Phys. Rev. Lett.* **68**, 21 (1992).
- [3] P. Camus, S. Cohen, L. Pruvost, and A. Bolovinos, *Phys. Rev. A* **48**, R9 (1993).
- [4] P. Camus, T. F. Gallagher, J. M. Lecomte, P. Pillet, L. Pruvost, and J. Boulmer, *Phys. Rev. Lett.* **62**, 2365 (1989).
- [5] U. Eichmann, V. Lange, and W. Sandner, *Phys. Rev. Lett.* **64**, 274 (1990).
- [6] S. N. Pisharody and R. R. Jones, *Science* **303**, 813 (2004).
- [7] X. Zhang, R. R. Jones, and F. Robicheaux, *Phys. Rev. Lett.* **110**, 023002 (2013).
- [8] T. F. Gallagher, *Rydberg Atoms* (Cambridge University Press, Cambridge, 1994).
- [9] M. Aymar, C. H. Greene, and E. Luc-Koenig, *Rev. Mod. Phys.* **68**, 1015 (1996).
- [10] M. Génévriez, *Mol. Phys.* **119**, e1861353 (2021).
- [11] M. Génévriez, C. Rosen, and U. Eichmann, *Phys. Rev. A* **104**, 012812 (2021).
- [12] U. Eichmann, T. F. Gallagher, and R. M. Konik, *Phys. Rev. Lett.* **90**, 233004 (2003).
- [13] U. Fano, *Phys. Rev.* **124**, 1866 (1961).
- [14] U. Eichmann, T. F. Gallagher, and R. M. Konik, *Phys. Rev. Lett.* **94**, 229302 (2005).
- [15] J. W. Cooper, C. H. Greene, P. W. Langhoff, A. F. Starace, and C. L. Winstead, *Phys. Rev. Lett.* **94**, 229301 (2005).
- [16] H. S. Margolis, G. Huang, G. P. Barwood, S. N. Lea, H. A. Klein, W. R. C. Rowley, P. Gill, and R. S. Windeler, *Phys. Rev. A* **67**, 032501 (2003).
- [17] N. L. S. Martin, D. B. Thompson, R. P. Bauman, C. D. Caldwell, M. O. Krause, S. P. Frigo, and M. Wilson, *Phys. Rev. Lett.* **81**, 1199 (1998).
- [18] B. Krässig, E. P. Kanter, S. H. Southworth, R. Guillemin, O. Hemmers, D. W. Lindle, R. Wehlitz, and N. L. S. Martin, *Phys. Rev. Lett.* **88**, 203002 (2002).
- [19] A. Muni, L. Lachaud, A. Couto, M. Poirier, R. C. Teixeira, J.-M. Raimond, M. Brune, and S. Gleyzes, *Nat. Phys.* **18**, 502 (2022).
- [20] U. Eichmann, P. Brockmann, V. Lange, and W. Sandner, *J. Phys. B: At. Mol. Opt. Phys.* **22**, L361 (1989).
- [21] C. Rosen, M. Dörr, U. Eichmann, and W. Sandner, *Phys. Rev. Lett.* **83**, 4514 (1999).
- [22] R. R. Freeman and D. Kleppner, *Phys. Rev. A* **14**, 1614 (1976).
- [23] Y. Komninos and C. A. Nicolaides, *Phys. Rev. A* **70**, 042507 (2004).
- [24] W. E. Cooke, T. F. Gallagher, S. A. Edelstein, and R. M. Hill, *Phys. Rev. Lett.* **40**, 178 (1978).
- [25] M. Génévriez, D. Wehrli, and F. Merkt, *Phys. Rev. A* **100**, 032517 (2019).
- [26] D. Wehrli, M. Génévriez, and F. Merkt, *Phys. Rev. A* **100**, 012515 (2019).
- [27] B. Simon, *Phys. Lett. A* **71**, 211 (1979).
- [28] C. A. Nicolaides and D. R. Beck, *Phys. Lett. A* **65**, 11 (1978).
- [29] T. N. Rescigno and C. W. McCurdy, *Phys. Rev. A* **62**, 032706 (2000).
- [30] T. N. Rescigno and V. McKoy, *Phys. Rev. A* **12**, 522 (1975).
- [31] R. D. Cowan, in *The Theory of Atomic Structure and Spectra*, Los Alamos Series in Basic and Applied Sciences (University of California Press, Berkeley, 1981), Chap. 13, p. 358.
- [32] S. A. Bhatti, C. L. Cromer, and W. E. Cooke, *Phys. Rev. A* **24**, 161 (1981).
- [33] J. W. Cooper, *Phys. Rev.* **128**, 681 (1962).
- [34] H. A. Bethe and E. E. Salpeter, *Quantum Mechanics of One- and Two-Electron Atoms* (Plenum, New York, 1977).
- [35] S. Pasternack and R. M. Sternheimer, *J. Math. Phys.* **3**, 1280 (1962).
- [36] W. E. Cooke and C. L. Cromer, *Phys. Rev. A* **32**, 2725 (1985).
- [37] L. D. Van Woerkom and W. E. Cooke, *Phys. Rev. A* **37**, 3326 (1988).
- [38] A. Giusti-Suzor and U. Fano, *J. Phys. B: At. Mol. Phys.* **17**, 215 (1984).
- [39] S. A. Bhatti and W. E. Cooke, *Phys. Rev. A* **28**, 756 (1983).
- [40] J. G. Story and W. E. Cooke, *Phys. Rev. A* **39**, 4610 (1989).
- [41] R. P. Wood and C. H. Greene, *Phys. Rev. A* **49**, 1029 (1994).
- [42] V. Letchumanan, M. A. Wilson, P. Gill, and A. G. Sinclair, *Phys. Rev. A* **72**, 012509 (2005).
- [43] W. Huang, C. Rosen, U. Eichmann, and W. Sandner, *Phys. Rev. A* **61**, 040502(R) (2000).
- [44] R. C. Teixeira, A. Larrouy, A. Muni, L. Lachaud, J.-M. Raimond, S. Gleyzes, and M. Brune, *Phys. Rev. Lett.* **125**, 263001 (2020).
- [45] A. P. Burgers, S. Ma, S. Saskin, J. Wilson, M. A. Alarcón, C. H. Greene, and J. D. Thompson, *PRX Quantum* **3**, 020326 (2022).
- [46] K.-L. Pham, T. F. Gallagher, P. Pillet, S. Lepoutre, and P. Cheinet, *PRX Quantum* **3**, 020327 (2022).
- [47] A. Kramida, Y. Ralchenko, and J. Reader, NIST Atomic Spectra Database (version 5.8), 2020, <https://doi.org/10.18434/T4W30F>.
- [48] S. Weber, C. Tresp, H. Menke, A. Urvoy, O. Firstenberg, H. P. Büchler, and S. Hofferberth, *J. Phys. B: At. Mol. Opt. Phys.* **50**, 133001 (2017).